Phase separation in a t-J model

M. Marder,* N. Papanicolaou,† and G. C. Psaltakis
Department of Physics, University of Crete, 71409 Iraklion, Greece
and Research Center of Crete, 71409 Iraklion, Greece
(Received 13 October 1989)

We study a simple extension of the Heisenberg model that is abstracted from the large-U limit of the Hubbard Hamiltonian and includes charge fluctuations. An attempt is made to elucidate some basic features of the $T=0$ phase diagram within a suitable $1/N$ expansion. We find that the ferromagnetic boundary dictated by a naive application of the Nagaoka theorem is actually incorrect because of an instability induced by phase separation. We derive what we believe to be the correct ferromagnetic boundary for sufficiently high dimension, and provide a detailed description of the ensuing phase separation. We also find that a uniform canted antiferromagnetic state is stable over a nontrivial region of the phase diagram. Potential implications of these results for the physics of the original Hubbard model are briefly discussed.

I. INTRODUCTION

The Hubbard model has recently received renewed interest in view of potential applications to the theory of high-T_c superconductivity. Nonetheless, many fundamental aspects of its solution remain elusive, with the notable exception of an exact solution available in one dimension through the Bethe ansatz.[1] The only rigorous result thought to be applicable to higher dimensions is a theorem due to Nagaoka,[2] whose implications have often been exaggerated in the literature. As a consequence, even the gross features of the $T=0$ phase diagram have not been firmly established, except in one dimension where the ground state is a spin singlet for arbitrary electron filling.

In order to achieve a manageable theoretical framework, the original Hubbard model is simplified in two respects. First, we restrict attention to the currently popular t-J model. Second, we partially alter the commutation relations of the Hubbard operators. The t-J model may be obtained as the large-U limit of the Hubbard model,[3] and is most conveniently formulated in terms of the Hubbard operators $\chi^{ab}=|a\rangle\langle b|$. Because double occupancy is projected out in the large-U limit, the Latin indices $a,b,\ldots$ assume only three distinct values, say 0, 1, and 2, corresponding to a hole, a spin-up electron, and a spin-down electron, respectively. We also use Greek indices $\mu,\nu,\ldots$ taking the two distinct values 1 and 2, and invoke the usual summation convention for repeated indices without exception. With these conventions the t-J Hamiltonian is written as

$$\begin{aligned}
&\mathcal{H}=\mathcal{H}_1+\mathcal{H}_2+\mathcal{H}_3 ,\\
&\mathcal{H}_1=-\sum_{i,j} t_{ij}\chi_i^{0\mu}\chi_j^{\mu 0} ,\\
&\mathcal{H}_2=\frac{1}{U}\sum_{i,j} t_{ij}^2(\chi_i^{\mu\nu}\chi_j^{\nu\mu}-\chi_i^{\mu\mu}\chi_j^{\nu\nu}) ,\\
&\mathcal{H}_3=\frac{1}{U}\sum_{\substack{i,l,j\\(i\neq j)}} t_{il}t_{lj}(\chi_i^{0\mu}\chi_l^{\mu\nu}\chi_j^{\nu 0}-\chi_i^{0\mu}\chi_l^{\nu\nu}\chi_j^{\mu 0}) ,
\end{aligned} \tag{1.1}$$

where we allow for arbitrary hopping constants $t_{ij}=t_{ji}$. In our explicit calculations hopping is assumed to occur only between neighboring sites with amplitude t. Hence the term $\mathcal{H}_1$ in (1.1) describes exchanges of holes with electrons occupying neighboring sites, whereas the three-site term $\mathcal{H}_3$ induces exchanges of holes with nearby pairs of electrons of opposite spin. The physical significance of $\mathcal{H}_2$ becomes apparent by expressing it in terms of the spin operators

$$\mathbf{S}_l=\tfrac{1}{2}\boldsymbol{\sigma}_{\mu\nu}\chi_l^{\mu\nu} , \tag{1.2}$$

where the $\boldsymbol{\sigma}_{\mu\nu}$ are matrix elements of the Pauli operators $\boldsymbol{\sigma}=(\sigma^x,\sigma^y,\sigma^z)$. A short calculation shows that $\mathcal{H}_2$ is essentially the usual antiferromagnetic Heisenberg Hamiltonian with exchange constant $J=4t^2/U$. The hopping constant t and exchange constant J will be used as the independent coupling constants in all subsequent calculations. In particular, we will frequently use the dimensionless ratio $t/J=U/(4t)$.

The Hamiltonian (1.1) must be supplemented by the local constraint

$$\chi_l^{aa}=\chi_l^{00}+\chi_l^{\mu\mu}=1 , \tag{1.3}$$

which expresses the fact that a site l is either empty or occupied by no more than one electron of arbitrary spin, and by the global constraint

$$\sum_l \chi_l^{\mu\mu}=N_e=n_e\Lambda , \tag{1.4}$$

where N_e is the total number of electrons and Λ is the total number of sites. The average density $n_e=N_e/\Lambda$ is referred to as the filling factor and will take values in $[0,1]$. A method for resolving the local constraint (1.3) will be described in Sec. II while the global constraint (1.4) will be treated by means of a chemical potential.

To complete the description of the Hamiltonian we must examine the commutation relations satisfied by the Hubbard operators. From their definition, $\chi^{ab}=|a\rangle\langle b|$, the Hubbard operators at any given site satisfy the U(3) algebra

$$[\chi_l^{ab},\chi_l^{cd}]=\delta^{bc}\chi_l^{ad}-\delta^{ad}\chi_l^{cb}\ , \tag{1.5}$$

where $[\ldots,\ldots]$ denotes the usual commutator. Although anticommutators do not occur in (1.5) the Fermi character of the original degrees of freedom is completely taken into account by the compactness of the unitary algebra U(3). However, operators at different sites may commute or anticommute depending on the specific choice of indices. For instance, $\chi_i^{0\mu}$ anticommutes with $\chi_j^{0\nu}$ if $i\neq j$ while it commutes with $\chi_j^{\mu\nu}$ or χ_j^{00}. This brings us to the second simplification of the Hubbard model; namely, operators at different sites will always be assumed to commute. Combining this simplification with the commutation relations (1.5), which remain intact, the general commutation relations will be written as

$$[\chi_i^{ab},\chi_j^{cd}]=\delta_{ij}(\delta^{bc}\chi_i^{ad}-\delta^{ad}\chi_i^{cb})\ . \tag{1.6}$$

It is difficult at this point to gauge the effect of altering the commutation relations. This model defines a simple extension of the Heisenberg model which includes charge fluctuations, containing most if not all the essential physics of the standard $t-J$ model, and perhaps of the original Hubbard model as well. We will study this model in its own right. The main advantage of the partial bosonization incorporated in (1.6) is that we are now able to develop a complete semiclassical theory in close analogy with earlier work on quantum-spin-1 systems.[4] In particular, we preserve the local constraint (1.3) exactly at each order of perturbation theory.

Thus we attempt to elucidate some basic features of the phase diagram of the Hubbard model. We find that the ferromagnetic boundary dictated by a naive application of the Nagaoka theorem is actually incorrect because of an instability induced by phase separation. We derive what we believe to be the correct ferromagnetic boundary for sufficiently high lattice dimension, and provide a detailed description of the ensuing phase separation. We also find that a canted antiferromagnetic state may be stable over a nontrivial region of the phase diagram.

In the course of our investigation, we learned that general arguments in favor of phase separation had already been given in an early paper by Visscher,[5] and in recent works by Ioffe and Larkin,[6] and Foerster.[7] Related ideas may also be found in articles on spin polarons[8] and on spin bags.[9] But we believe that our present work contains the first attempt to develop the scenario of phase separation in correlated electron systems with reasonable completeness.

The needed formalism is adapted to the present problem in Sec. II. The resulting semiclassical theory is then employed in Sec. III to study the ground state of our model, its elementary excitations (magnons and holons), and its phase diagram. While the main results of Sec. III are obtained by means of simple analytical arguments, their detailed justification rests in part upon numerical experiments. In one dimension, a rigorous justification of the main results is possible using a transfer-matrix technique described in Sec. IV. Our conclusions are summarized in Sec. V.

II. SEMICLASSICAL THEORY

The model defined in the preceding section may be viewed as a pseudospin system whose Hamiltonian is expressed in terms of the generators of the unitary algebra U(3). The purpose of this section is to describe a semiclassical theory which is a relatively straightforward generalization of the well-known theory of the ordinary Heisenberg model. Since the details of this approach have already been discussed in the context of quantum-spin-1 systems,[4] our description here will be brief.

The local constraint (1.3) indicates that the relevant representation of U(3) is the fundamental (quark) representation. To derive a sensible semiclassical theory we generalize the constraint according to

$$\chi_l^{aa}=\chi_l^{00}+\chi_l^{\mu\mu}=N\ , \tag{2.1}$$

where N, not to be confused with the electron number N_e, is arbitrary. From the algebraic point of view (2.1) is equivalent to asserting that we consider an arbitrary symmetric representation of U(3) by analogy with the generalization of the spin-$\frac{1}{2}$ Heisenberg model to arbitrary spin S. Of course, the global constraint (1.4) should be modified accordingly:

$$\sum_l \chi_l^{\mu\mu}=n_e N\Lambda\ . \tag{2.2}$$

One may then derive a semiclassical theory based on a $1/N$ expansion, along the lines of the $1/S$ expansion extensively used in the study of the Heisenberg model, setting $N=1$ at the end of the calculation. In order to appreciate fully the semiclassical nature of the large-N limit, one should proceed with the derivation of a phase-space path integral in terms of generalized coherent states for the symmetric representations of the unitary algebra.[4] However, for most practical purposes, the essential results are (i) a generalized Holstein-Primakoff approach suitable for the study of the low-temperature dynamics and (ii) a certain classical approximation to the partition function that may be used for the study of phase transitions and related issues.

The generalized Holstein-Primakoff realization at site l is given by

$$\chi_l^{00}=N-\xi_l^{\mu *}\xi_l^{\mu},\quad \chi_l^{\mu\nu}=\xi_l^{\mu *}\xi_l^{\nu}\ , \tag{2.3}$$

$$\chi_l^{0\mu}=(N-\xi_l^{\nu *}\xi_l^{\nu})^{1/2}\xi_l^{\mu},\quad \chi_l^{\mu 0}=\xi_l^{\mu *}(N-\xi_l^{\nu *}\xi_l^{\nu})^{1/2}\ ,$$

where the ξ_l^{μ} are Bose operators;

$$[\xi_i^{\mu},\xi_j^{\nu *}]=\delta_{ij}\delta^{\mu\nu}\ . \tag{2.4}$$

One can verify by a direct calculation that the operators in (2.3) satisfy the unitary algebra (1.6) for all partitions of indices, by virtue of the Bose algebra (2.4). It is also clear that the local constraint (2.1) has been explicitly resolved in (2.3). Finally the bosonized expressions for the local electron density N_l and the spin operators $\mathbf{S}_l$ are given by

$$N_l=\xi_l^{\mu *}\xi_l^{\mu},\quad \mathbf{S}_l=\tfrac{1}{2}\boldsymbol{\sigma}_{\mu\nu}\xi_l^{\mu *}\xi_l^{\nu}\ . \tag{2.5}$$

Inserting (2.3) into (1.1) yields a completely bosonized effective Hamiltonian which is suitable for the study of low-temperature dynamics using standard spin-wave techniques. An essential step in this approach is to determine the minimum of the effective Hamiltonian in the large-N limit, where the operators ξ_l^μ may be treated as classical (commuting) fields. To make the semiclassical nature of the large-N limit explicit one may introduce rescaled operators ζ_l^μ from

$$\xi_l^\mu = N^{1/2}\zeta_l^\mu, \quad [\zeta_l^\mu, \zeta_j^{\nu *}] = \frac{1}{N}\delta_{ij}\delta^{\mu\nu} , \tag{2.6}$$

whose commutator vanishes for large N. Note also that N factors out nicely when the ζ_l^μ are introduced into the Holstein-Primakoff realization (2.3);

$$\chi_l^{00} = N(1-\zeta_l^{\mu *}\zeta_l^\mu), \quad \chi_l^{\mu\nu} = N\zeta_l^{\mu *}\zeta_l^\nu ,$$
$$\chi_l^{0\mu} = N(1-\zeta_l^{\nu *}\zeta_l^\nu)^{1/2}\zeta_l^\mu, \quad \chi_l^{\mu 0} = N\zeta_l^{\mu *}(1-\zeta_l^{\nu *}\zeta_l^\nu)^{1/2} . \tag{2.7}$$

Similarly, the charge and spin densities of (2.5) will be written as

$$N_l = Nn_l, \quad n_l = \zeta_l^{\mu *}\zeta_l^\mu ,$$
$$\mathbf{S}_l = N\mathbf{s}_l, \quad \mathbf{s}_l = \tfrac{1}{2}\boldsymbol{\sigma}_{\mu\nu}\zeta_l^{\mu *}\zeta_l^\nu . \tag{2.8}$$

Since $N=1$ will eventually be the value of actual interest, the densities N_l and $\mathbf{S}_l$ will ultimately be indistinguishable from n_l and $\mathbf{s}_l$.

Treating ζ_l as a commuting field in the large-N limit, we may parametrize it so as to reveal the underlying rotational invariance by writing

$$\zeta_l^1 = n_l^{1/2} e^{i\psi_l}\cos\left(\frac{\theta_l}{2}\right)e^{-i\phi_l/2} ,$$
$$\zeta_l^2 = n_l^{1/2} e^{i\psi_l}\sin\left(\frac{\theta_l}{2}\right)e^{i\phi_l/2} . \tag{2.9}$$

Thus the spin density at site l takes on the usual spherical parametrization

$$s_l^x = \tfrac{1}{2}n_l\sin\theta_l\cos\phi_l ,$$
$$s_l^y = \tfrac{1}{2}n_l\sin\theta_l\sin\phi_l , \tag{2.10}$$
$$s_l^z = \tfrac{1}{2}n_l\cos\theta_l .$$

These expressions also reveal that to leading order the magnitude of the local spin is one-half of the local charge density.

The large-N classical energy is calculated by inserting (2.7) into the Hamiltonian and by neglecting the ordering of the operators. The resulting energy function will be written here symbolically as

$$\mathcal{E} = \mathcal{E}(\zeta^*, \zeta) = \mathcal{E}(n, \psi, \theta, \phi) , \tag{2.11}$$

and our first task will be to minimize this function with respect to the classical complex variables ζ_l^μ, or the spherical variables (2.9). It should be noted that this minimization problem is equivalent to a Hartree variational calculation except that higher-order corrections may now be computed through a systematic $1/N$ expansion around the classical minimum of (2.11).

The explicit calculation of the classical minimum turns out to be more difficult than we had expected and will occupy most of our effort in this paper. This situation should be contrasted with the corresponding one in the Heisenberg model, where the determination of the classical minimum is straightforward; the minimum occurs when all spins are aligned, in the case of a ferromagnet, or for a Néel lattice, in the case of an antiferromagnet.

To complete the general description of the semiclassical theory we note that the classical energy (2.11) may also be used to construct a certain classical approximation to the partition function, namely

$$Z_{\rm cl} = \int \prod_{\mu,l} d^2\zeta_l^\mu e^{-\beta\mathcal{E}}$$
$$= \int \prod_l \left(\tfrac{1}{8}n_l dn_l \sin\theta_l d\theta_l d\phi_l d\psi_l\right) e^{-\beta\mathcal{E}} , \tag{2.12}$$

where the integration at each site l extends over the finite disk $\zeta_l^{\mu *}\zeta_l^\mu \le 1$, with $d^2\zeta$ denoting integration over both real and imaginary parts of the complex variables ζ, or over the intervals $0 \le n_l \le 1$, $0 \le \theta_l \le \pi$, $0 \le \phi_l \le 2\pi$, and $0 \le \psi_l \le 2\pi$. The classical energy in (2.12) should also include a chemical potential to account for the global constraint (2.2).

Drawing on long experience with the Heisenberg model, one would expect the classical model defined by (2.12) to be in the same universality class with the original quantum model. Putting it differently, the nature of the phase transitions as well as the explicit values of the critical exponents derived from (2.12) should coincide with those of the quantum t-J model. Of course, an explicit calculation of (2.12) is still a difficult problem; this is discussed further in Sec. IV.

Thus we have outlined a complete semiclassical theory for the quantum t-J model defined in Sec. I, with all the virtues and weaknesses of the corresponding theory in the ordinary Heisenberg model. The main advantage of this approach is that both low- and high-temperature thermodynamics, as well as intervening phase transitions, may be studied without unreasonable effort. The main weakness is that a semiclassical theory such as this one tends to exaggerate the possibility of ordering, and, while typically correct in three or more dimensions, may fail in two or less. However, recent experience with the two-dimensional quantum antiferromagnet suggests that a semiclassical approach can prove useful even in low dimension.

III. PHASE SEPARATION

Our immediate goal is to find the collection of ζ_l^μ which minimizes the classical energy $\mathcal{E}(\zeta^*, \zeta)$. We will for the moment neglect the three-site term $\mathcal{H}_3$ in the Hamiltonian (1.1). This restriction simplifies the analysis while preserving the essential physical picture. Later in this section we will see how the picture is modified by the reintroduction of $\mathcal{H}_3$.

We obtain an explicit expression for the classical energy by inserting (2.7) into $\mathcal{H}=\mathcal{H}_1+\mathcal{H}_2$ and by neglecting the ordering of the operators:

$$\begin{aligned}\mathcal{E}&=\mathcal{E}_1+\mathcal{E}_2\ ,\\ \mathcal{E}_1&=-N^2t\sum_{\langle ij\rangle}[(1-\xi_i^{\mu*}\xi_i^{\mu})(1-\xi_j^{\nu*}\xi_j^{\nu})]^{1/2}\\ &\quad\times(\xi_i^{\lambda*}\xi_j^{\lambda}+\xi_j^{\lambda*}\xi_i^{\lambda})\ ,\\ \mathcal{E}_2&=\tfrac{1}{2}N^2J\sum_{\langle ij\rangle}[|\xi_i^{\mu*}\xi_j^{\mu}|^2-(\xi_i^{\mu*}\xi_i^{\mu})(\xi_j^{\nu*}\xi_j^{\nu})]\ .\end{aligned}\tag{3.1}$$

Here $\langle ij\rangle$ denotes summation over neighboring sites, and $J=4t^2/U$ is the exchange constant. The overall factor N^2 is important only to distinguish the semiclassical approximation from higher-order $1/N$ corrections. With this understanding, N will be set equal to the value of actual interest ($N=1$) in the following calculations. It will also prove convenient to work with the spherical variables given in (2.9) so that the energy is written as

$$\begin{aligned}\mathcal{E}_1&=-2t\sum_{\langle ij\rangle}[n_i(1-n_i)n_j(1-n_j)]^{1/2}\left[\cos\frac{\theta_i}{2}\cos\frac{\theta_j}{2}\cos\left[\psi_i-\psi_j-\frac{\phi_i-\phi_j}{2}\right]+\sin\frac{\theta_i}{2}\sin\frac{\theta_j}{2}\cos\left[\psi_i-\psi_j+\frac{\phi_i-\phi_j}{2}\right]\right]\ ,\\ \mathcal{E}_2&=\tfrac{1}{4}J\sum_{\langle ij\rangle}n_in_j[\cos\theta_i\cos\theta_j+\cos(\phi_i-\phi_j)\sin\theta_i\sin\theta_j-1]\ .\end{aligned}\tag{3.2}$$

The global constraint (2.2) will be treated by means of a chemical potential μ, so we must find extrema of the function

$$\mathcal{F}=\mathcal{E}_1+\mathcal{E}_2-\mu\sum_l(n_l-n_e)\ .\tag{3.3}$$

This minimization problem appears to be a difficult task. We will proceed by invoking certain simplifying assumptions whose validity will be examined at later states of our discussion. We first assume that the phases ψ_l and azimuthal angles ϕ_l are uniform, so we may set $\psi_i-\psi_j=0=\phi_i-\phi_j$ in (3.2) to obtain

$$\begin{aligned}\mathcal{E}&=\mathcal{E}_1+\mathcal{E}_2\ ,\\ \mathcal{E}_1&=-2t\sum_{\langle ij\rangle}[n_i(1-n_i)n_j(1-n_j)]^{1/2}\cos\left[\frac{\theta_i-\theta_j}{2}\right]\ ,\\ \mathcal{E}_2&=-\frac{J}{2}\sum_{\langle ij\rangle}n_in_j\sin^2\left[\frac{\theta_i-\theta_j}{2}\right]\ .\end{aligned}\tag{3.4}$$

The minimization problem remains difficult, but some insight can be gained by examining $\mathcal{E}_1$ and $\mathcal{E}_2$ individually. Notice that $\mathcal{E}_1$ would achieve its minimum value when spins are parallel ($\theta_i-\theta_j=0$) whereas $\mathcal{E}_2$ would be minimized when the spins at neighboring sites are antiparallel ($\theta_i-\theta_j=\pi$.) In particular, in the limit of a half-filled band ($n_e=1$), the energy $\mathcal{E}_1+\mathcal{E}_2$ achieves its minimum value when the spins form the usual Néel lattice because the hopping energy $\mathcal{E}_1$ is then suppressed. Looking for a configuration able to interpolate between ferromagnetism and antiferromagnetism, we assume (i) a uniform electron density; $n_l=n_e$ on all sites, and (ii) a bipartite lattice with a constant angular difference $\theta_i-\theta_j=\pm\theta_c$ between neighboring sites i and j. The *canting angle* θ_c should reduce to $\theta_c=\pi$ at $n_e=1$, and $\theta_c=0$ at $n_e=0$.

Incorporating these assumptions into (3.4) one finds that

$$\mathcal{E}/\Lambda=-ztn_e(1-n_e)\cos\frac{\theta_c}{2}-\tfrac{1}{4}zJn_e^2\sin^2\frac{\theta_c}{2}\ ,\tag{3.5}$$

where Λ is the total number of sites, and z is the lattice coordination number.

As it turns out, the first assumption is not actually justified, but it is instructive to follow this line of reasoning through to its conclusion. Minimizing (3.5) with respect to θ_c we find that

$$\cos\left[\frac{\theta_c}{2}\right]=\begin{cases}2\dfrac{t}{J}\dfrac{1-n_e}{n_e}, & \text{for } t/J\le\dfrac{n_e}{2(1-n_e)}\ ;\\ 1, & \text{for } t/J\ge\dfrac{n_e}{2(1-n_e)}\end{cases}\ .\tag{3.6}$$

Therefore a critical line develops in the n_e-t/J plane, given by

$$\frac{t}{J}=\frac{n_e}{2(1-n_e)}\ ,\tag{3.7}$$

and drawn as a dashed line in Fig. 1. Above the critical

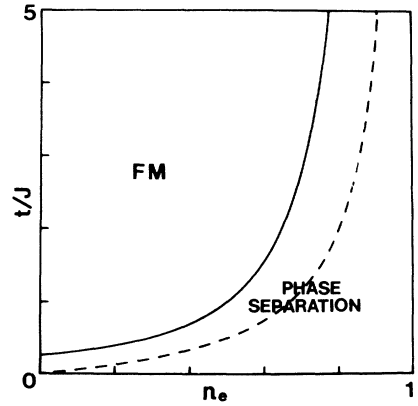

FIG. 1. $T=0$ phase diagram in the absence of $\mathcal{H}_3$. The dashed line indicates the limit of metastability defined in Eq. (3.7), whereas the solid line is the true critical line of Eq. (3.12). Above the critical line the system orders ferromagnetically (FM), while it undergoes phase separation in the remaining region.

line, the system orders ferromagnetically. The destruction of perfect ferromagnetism at the line is consistent with the usual interpretation of Nagaoka's original calculation. Below the line, the system forms a canted phase which interpolates smoothly between ferromagnetism ($\theta_c=0$) and antiferromagnetism ($\theta_c=\pi$) at half filling ($n_e=1$).

The ground-state energy is given by

$$\mathcal{E}/zt\Lambda=\begin{cases}-\frac{t}{J}(1-n_e)^2-\frac{J}{4t}n_e^2, & \text{for } t/J\le\frac{n_e}{2(1-n_e)}\ ;\\ -n_e(1-n_e), & \text{for } t/J\ge\frac{n_e}{2(1-n_e)}\ ,\end{cases}\tag{3.8}$$

and is a continuous function of n_e across the critical line. The chemical potential, $\mu=\mathcal{E}'(n_e)/\Lambda$, or

$$\frac{\mu}{zt}=\begin{cases}\frac{2t}{J}(1-n_e)-\frac{J}{2t}n_e, & \text{for } t/J\le\frac{n_e}{2(1-n_e)}\ ;\\ 2n_e-1 & \text{for, } t/J\ge\frac{n_e}{2(1-n_e)}\ ,\end{cases}\tag{3.9}$$

is also continuous. However, the second derivative, $\mathcal{E}''$ is discontinuous, a fact of importance to which we will return shortly.

In order to decide whether or not this classical configuration is a reasonable candidate for the ground state, we examine its local stability; that is, stability against small fluctuations. Such a calculation is possible by using a systematic $1/N$ expansion based on the machinery developed in Sec. II. One expands the Hamiltonian to quadratic order in quantum fluctuations about the classical configuration, and diagonalizes the resulting quadratic Hamiltonian. Here we describe only the final results for the spectrum of elementary excitations; these consist of a magnon, and a mode that accounts for charge fluctuations, which will be called a holon.

In the ferromagnetic phase, the magnon energy-momentum dispersion is given by

$$\omega_k=z[(1-n_e)t-\tfrac{1}{2}n_eJ](1-\gamma_k)\ ,\qquad \gamma_k\equiv\frac{1}{z}\sum_{\delta}e^{i\mathbf{k}\cdot\delta}\ ,\tag{3.10a}$$

where δ is summed over the z nearest neighbors. The corresponding holon dispersion reads

$$\Omega_k=zt\{(1-\gamma_k)[1-(1-2n_e)^2\gamma_k]\}^{1/2}\ .\tag{3.10b}$$

A careful inspection of the dispersions reveals no sign of instability for values of the parameters in the region above the critical line (3.7). The magnon energy ω_k vanishes at the critical line and eventually becomes negative. Of course, such a result is consistent with our earlier analysis which suggested a canted phase below the critical line. To check the stability of the canted phase, we have again calculated the spectrum of the corresponding elementary excitations. After a long calculation, the magnon energy is found to be

$$\omega_k=\tfrac{1}{2}zn_e\left[(1-\gamma_k)\left\{J^2(1-\gamma_k\cos\theta_c)+4t^2(1-\gamma_k)\cos^2\frac{\theta_c}{2}+4tJ(1+\gamma_k)\cos\frac{\theta_c}{2}\right\}\right]^{1/2},\tag{3.11a}$$

where θ_c is the canting angle of (3.6). However, the holon dispersion vanishes identically for all momenta in the Brillouin zone:

$$\Omega_k=0,\quad \text{for all } k\ .\tag{3.11b}$$

Before analyzing the potentially interesting consequences of the last equation, we wish to discuss some consistency checks. At half filling ($n_e=1,\theta_c=\pi$), the magnon (3.11a) reduces to the usual antiferromagnetic magnon, as expected. At the critical line (3.7), the magnon (3.11a) of the canted phase coincides with the holon (3.10b) of the ferromagnetic phase. Similarly, the ferromagnetic magnon (3.10a) vanishes at the critical line and thus coincides with the holon (3.11b) of the canted phase. This transmutation of modes across the critical line reflects strong hybridization between charge and spin degrees of freedom. In particular, one should expect that both magnons and holons contribute, with appropriate weights, to physical quantities such as magnetic susceptibility, optical conductivity, and so on.

Although it may appear that we have obtained a satisfactory account of the ferromagnetic and canted phases, the peculiar (vanishing) holon mode (3.11b) indicates that there may be trouble lurking beneath the surface. It is worth remarking that a similar mode occurs within a $1/N$ expansion of a different nature used in the study of the ordinary quantum antiferromagnet.[10] The appearance of a mode whose energy vanishes throughout the Brillouin zone to quadratic order leaves open the question of local stability. Also open remains the question of global stability, for the simple semiclassical ground state we have proposed could in principle be unstable to multimagnon or multiholon processes. Both of these questions could in principle be settled by a detailed examination of higher-order (anharmonic) $1/N$ corrections.

In fact, the issue of stability can be settled by simple arguments based on the convexity of the ground-state energy $\mathcal{E}=\mathcal{E}(n_e)$, which appeared in Eq. (3.8). Our subsequent analysis will show that the canted phase is actually everywhere unstable against long-wavelength fluctuations. And, while the ferromagnetic phase is locally stable, it becomes globally unstable over a nontrivial region of the phase diagram. The true critical line will be shown to be given by

$$\frac{t}{J}=\frac{1}{4(1-n_e)^2}\ ,\tag{3.12}$$

instead of Eq. (3.7), and is depicted by a solid line in Fig. 1. Above the true critical line, the system is indeed realized in a ferromagnetic phase which is both locally and globally stable. Below the true critical line, the system undergoes phase separation. In the space between solid

and dashed lines in Fig. 1, a ferromagnetic phase would be metastable.

The simplest route to Eq. (3.12) proceeds with an examination of the second derivative of the ground-state energy $\mathcal{E}=\mathcal{E}(n_e)$ of Eq. (3.8);

$$\mathcal{E}''(n_e)/zt\Lambda=\begin{cases}-\dfrac{2t}{J}-\dfrac{J}{2t}, & \text{for } t/J\le\dfrac{n_e}{2(1-n_e)}\ ;\\ 2, & \text{for } t/J\ge\dfrac{n_e}{2(1-n_e)}\ .\end{cases}\tag{3.13}$$

The second derivative is negative for $t/J<n_e/2(1-n_e)$. This guarantees that the energy of Eq. (3.8) is concave in the canted phase. An argument going back to Maxwell and Gibbs[11] asserts that the free energy of a system must always be a convex function of density: Otherwise, one can always construct a phase-separated state of lower free energy, and whose free energy is (marginally) convex.

An explicit demonstration of Maxwell's argument, as applied to the present case, is summarized by the geometrical construction of Fig. 2. The lower half of the figure shows the energy, Eq. (3.8), as a function of n_e at fixed t/J. In our particular example, we take $t/J=2.5$. The energy (3.8) is depicted in part by a dashed line, curve ABC, where it is concave. Point B shows where the ferromagnetic phase should end according to the early estimate, Eq. (3.7). Point A shows the location of the true phase boundary, given by Eq. (3.12). Let us compare the energy of a uniform-charge-density state that sits upon this dashed curve with one that involves macroscopic phase separation. If a fraction m of the system has charge density n_+, and a fraction $1-m$ of the system has density n_-, with $n_+>n_-$ and

$$mn_+ +(1-m)n_-=n_e\ ,\tag{3.14}$$

then the energy of a phase-separated state is

$$\mathcal{E}_{\rm PS}=m\mathcal{E}(n_+)+(1-m)\mathcal{E}(n_-)\ ,\tag{3.15}$$

where $\mathcal{E}(n_\pm)$ is the value of the energy (3.8) at $n_e=n_\pm$. Note that the interface energy is ignored in (3.15), as is appropriate in the thermodynamic limit.

Viewed as a function of n_e, the energy of the phase-separated configuration given in Eq. (3.15) is a straight line connecting the points $(n_-,\mathcal{E}(n_-))$ and $(n_+,\mathcal{E}(n_+))$. One chooses n_+ and n_- so that the straight line connecting these points lies as low as possible. This construction is illustrated by the solid line connecting points A and C in Fig. 2. One sees that $n_+=1$, so a fraction $m=(n_e-n_-)/(1-n_-)$ is purely antiferromagnetic. Again inspecting Fig. 2, one sees that at point A, the solid and dashed lines must be tangent to one another. This means that

$$\mathcal{E}'(n_-)=\frac{\mathcal{E}(n_+)-\mathcal{E}(n_-)}{n_+-n_-}\ ,\tag{3.16}$$

with $n_+=1$, while n_- lies somewhere in the ferromagnetic region. Expressing the energies appearing in (3.16) in units of $zt\Lambda$, Eq. (3.8) yields $\mathcal{E}(n_+)=\mathcal{E}(1)=-J/4t$, $\mathcal{E}(n_-)=-n_-(1-n_-)$, and $\mathcal{E}'(n_-)=2n_--1$. Inserting these expressions into Eq. (3.16) and solving for n_- we find that

$$n_+=1\ ,\qquad n_-=\begin{cases}1-\frac{1}{2}(J/t)^{1/2}, & \text{for } t/J>\frac{1}{4}\ ;\\ 0, & \text{for } t/J<\frac{1}{4}\ ,\end{cases}\tag{3.17}$$

which are the densities that correspond to optimal phase separation. Hence the ground-state configuration consists of a purely antiferromagnetic component with density $n_+=1$, and a purely ferromagnetic component of density n_-. Although the canted phase is the best configuration with uniform charge density for certain values of n_e, it is everywhere unstable against phase separation. However, the canted phase is stabilized to some extent by the inclusion of the three-site term in the Hamiltonian (1.1), a point to which we will return later in this section. The second equation in (3.17) is shown in the upper half of Fig. 2 as a solid line, and gives the true critical line announced earlier in Eq. (3.12) and in Fig. 1. To reveal an important feature of the true critical line, we write Eq. (3.12) as $J/t=4\delta^2$, where $\delta=1-n_e$ is the doping parameter. This quadratic dependence upon doping should be contrasted with the linear dependence suggested by Eq. (3.7), applied for small doping, or by naive inference from Nagaoka's calculation. Actually, arguments in favor of a critical line which behaves at small doping as $J/t\sim\delta^2$ have recently been given by Ioffe and

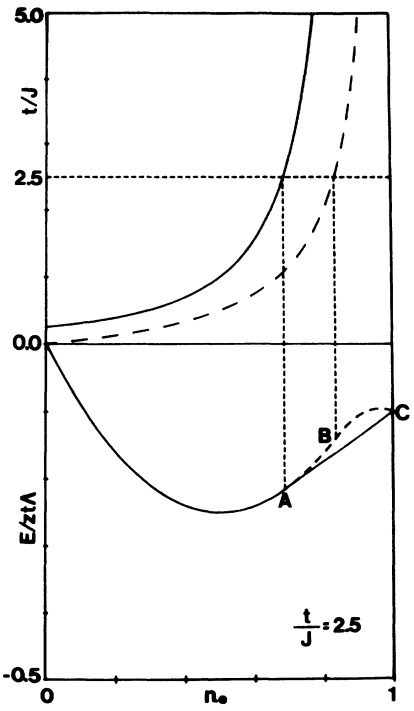

FIG. 2. Geometrical illustration of the Maxwell construction for phase separation; see the text for further explanation.

Larkin,[6] and by Foerster.[7] Here we provide an explicit expression for the critical line, as well as a detailed scenario for phase separation.

Notice also that for $t/J < \frac{1}{4}$ the system separates into a purely antiferromagnetic component, with $n_+ = 1$ and $m = n_e$, and a component consisting entirely of empty sites (holes). This feature is likely an artifact of the t-J model with no analog in the original Hubbard model, because the former is the large t/J limit of the latter.

To complete the picture, we must update the expressions for the ground-state energy and chemical potential given earlier in Eqs. (3.8) and (3.9);

$$\mathcal{E}/zt\Lambda = \begin{cases} [1-(J/t)^{1/2}]n_e - [1-\frac{1}{2}(J/t)^{1/2}]^2, & \text{for } t/J \le \dfrac{1}{4(1-n_e)^2} \ ; \\ -n_e(1-n_e), & \text{for } t/J \ge \dfrac{1}{4(1-n_e)^2} \ , \end{cases} \tag{3.18}$$

and

$$\mu/zt = \begin{cases} 1-(J/t)^{1/2}, & \text{for } t/J \le \dfrac{1}{4(1-n_e)^2} \ ; \\ 2n_e - 1, & \text{for } t/J \ge \dfrac{1}{4(1-n_e)^2} \ . \end{cases} \tag{3.19}$$

Note that the chemical potential remains constant for values of the density n_e in the region $n_- \le n_e \le 1$, where the system undergoes phase separation.

Although reasoning based upon the Maxwell construction establishes that the phase-separated configuration is lower in energy than the canted state, it falls short of proving that a configuration of still lower energy does not exist. An analytical proof that the phase-separated configuration is indeed the absolute minimum of the classical energy (3.1) has been possible in one dimension, and is presented in Sec. IV. We have not been able to obtain a similar proof in higher dimensions, but numerical experiments point to the same conclusion.

By a numerical experiment we mean a direct numerical minimization of the classical energy (3.1) or (3.2). Such a task is not entirely straightforward because of the large number of variables involved, especially for large lattice dimension. Hence most of our numerical calculations were based on the simpler form given in (3.4), which assumes that the overall phase ψ_l and the azimuthal angle ϕ_l are uniform at the minimum; this assumption implies, in particular, that all spins are contained in a plane. We have thus confirmed the heuristic picture derived above and obtained some additional insight concerning the nature of the interface separating the ferromagnetic and antiferromagnetic domains.

We have found that the classical energy possesses a multitude of local minima which correspond to formation of ferromagnetic or antiferromagnetic bubbles of varying size. Generically, these minima are metastable because the absolute minimum is achieved when the (positive) interface energy is minimized; this corresponds to the formation of exactly two domains, one ferromagnetic, the other antiferromagnetic. Bubbles attract each other with a strong but very short-ranged force and lower their energies when they unite. Examples of such bubbles are displayed in Fig. 3, and were obtained by a numerical minimization of (3.4) on a two-dimensional square lattice. Although it is difficult to discern from Fig. 3 the detailed nature of the interface, a more careful analysis shows that the interface is sharp on the antiferromagnetic side while it develops an exponential tail on the ferromagnetic side. One should also keep in mind that Fig. 3 was produced on the assumption that all spins lie in a plane. When this assumption is relaxed, spins on opposite sides of the interface might orient themselves perpendicular to one

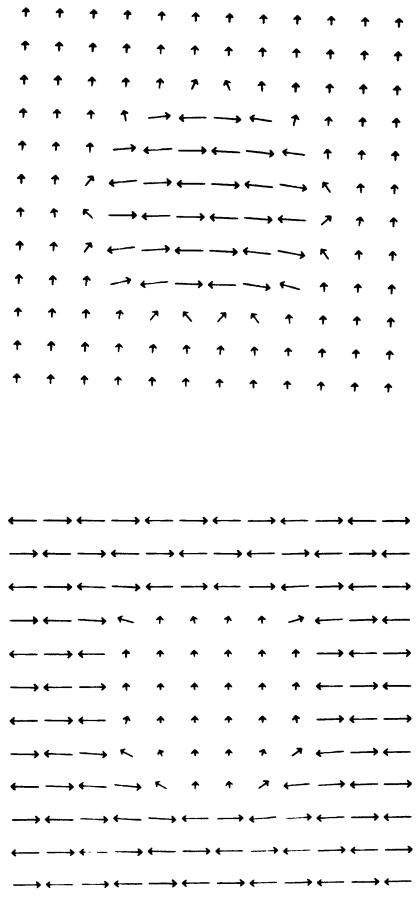

FIG. 3. Examples of antiferromagnetic and ferromagnetic bubbles obtained with a numerical minimization of the classical energy (3.4) on a square lattice.

another. A more detailed understanding of the interface is available in one dimension, and will be discussed in Sec. IV.

The formation of bubbles is reminiscent of earlier discussions of spin polarons[8] and spin bags.[9] In particular, holes are expelled from the antiferromagnetic region and cluster together within a ferromagnetic region of reduced charge density. Therefore, although an attraction between holes is clearly at work, it leads to the formation of macroscopic domains rather than to a conventional pairing. In this respect, the picture emerging here might be unfavorable for applications of the t-J model to the theory of high-T_c superconductivity.

Note that the phase diagram constructed above is independent of lattice dimension. One should recall that a similar situation arises in the ordinary Heisenberg model, where the Néel state is the lowest-energy semiclassical configuration in all dimension. On the other hand, the Néel state is certainly destroyed by quantum fluctuations in one dimension, while almost certainly being preserved in three dimensions. The situation in two dimensions is currently under debate, but the available evidence[12] suggests that long-range order is present at $T=0$.

Of course, it would be difficult to draw a precise analogy with the current model, but a few comments can be made. It is reasonable to assume that the phase separation obtained here through semiclassical arguments is an accurate description of the true (quantum) ground state at sufficiently large dimension D, perhaps as low as $D=3$. At the other extreme, $D=1$, quantum fluctuations do destroy magnetic order and lead to a ground state which is a spin singlet. Although it is unlikely that phase separation would occur within a singlet ground state, we have tested the well-known exact solution of the one-dimensional Hubbard model against the Maxwell and Gibbs criteria for stability. Shiba[13] has derived an expression for the ground-state energy in the large t/J limit, which is

$$\mathcal{E}/2t\Lambda \approx -\frac{\sin(\pi n_e)}{\pi} - \frac{J}{2t}(\ln 2) n_e^2 \left[1-\frac{\sin(2\pi n_e)}{2\pi n_e}\right] . \tag{3.20}$$

Interestingly, the first term is a convex function of n_e, while the second term is concave. In the large t/J limit, where the expression is valid, the first term dominates and leads to a convex total energy. Precisely at half filling, $n_e=1$, the second derivative of both terms vanishes, leaving room for speculation that the exact energy might be concave in the vicinity of $n_e=1$. Returning to the integral equations derived by Lieb and Wu,[1] we have computed the second derivative at $n_e=1$ for all t/J;

$$\mathcal{E}''(n_e=1)/2t\Lambda = \frac{2\int_{-\infty}^{\infty} d\omega \frac{1-J_0(\omega)}{1+e^{2|\omega| t/J}}}{1-\int_{-\infty}^{\infty} d\omega \frac{J_0(\omega)}{1+e^{2|\omega| t/J}}} , \tag{3.21}$$

where J_0 is the usual Bessel function. The right-hand side of (3.21) is always positive; thus, as expected, there is no phase separation in the one-dimensional Hubbard model. Similarly, it is unlikely that the (quantum) t-J model studied in this paper will exhibit phase separation in one dimension.

Therefore, when we say that phase separation is studied rigorously for the one-dimensional model in Sec. IV, we mean the classical t-J model, which exhibits phase separation at $T=0$ in all dimensions. Hence the work of Sec. IV studies one dimension to clarify features of phase separation which are only truly relevant to dimensions greater than one. Needless to say, we do not have at this point an estimate of the dimension above which phase separation occurs. In particular, we do not know whether or not the picture derived here is applicable in two dimensions.

We complete this section with a brief discussion of the effects resulting from the inclusion of the three-site term $\mathcal{H}_3$ in the Hamiltonian (1.1). Assuming as before that the charge density is uniform, we find the analog of (3.7), which gives the point at which a uniform ferromagnetic state is unstable against the formation of a uniform canted phase:

$$\frac{t}{G} = \frac{n_e}{2(1-n_e)} , \tag{3.22}$$

which has the same form as (3.7), except that the effective exchange constant G appearing in (3.22) is related to J by

$$G = J[1+(z-1)(1-n_e)] . \tag{3.23}$$

The explicit dependence of G on the coordination number z indicates that the phase diagram is no longer independent of lattice dimension, and its dependence on the charge density n_e will affect the stability analysis based on the second derivative of the energy.

The ground-state energy for uniform states [$\mathcal{E}=\mathcal{E}(n_e)$] is also obtained with the simple substitution $J \rightarrow G$ in Eq. (3.8). We have first examined the resulting energy as a function of n_e and located the regions where its second derivative is negative. An interesting deviation from our previous analysis is that the canted phase is now locally stable over some region of the phase diagram. This region is bounded from above by the curve (3.22), and by the curve

$$\frac{t}{J} = \tfrac{1}{2}[1+(z-1)(1-n_e)]^{3/2} [(3n_e-1)(z-1)-1]^{1/2} , \tag{3.24}$$

which is the curve on which the second derivative of the energy vanishes. As before, the energy remains concave for a nontrivial range of densities, so that the previous arguments lead to phase separation. It turns out that Eqs. (3.22) and (3.24) are not true critical lines, but indicate limits of metastability, drawn with dashed lines in Fig. 4 for various coordination numbers. By a geometrical construction similar to that presented in Fig. 2 we have located the true critical lines, which are the solid lines of Fig. 4.

For sufficiently large values of t/J, the true critical lines as well as the details of phase separation are identi-

cal to those described earlier in this section, in the absence of $\mathcal{H}_3$. This remark is especially important in view of the fact that the t-J model is the large t/J limit of the original Hubbard model. For lower values of t/J, deviations from the original picture depend upon lattice dimension. Hence a uniform canted phase is now possible on lattices with dimension greater than one, and there is more than one scenario for phase separation.

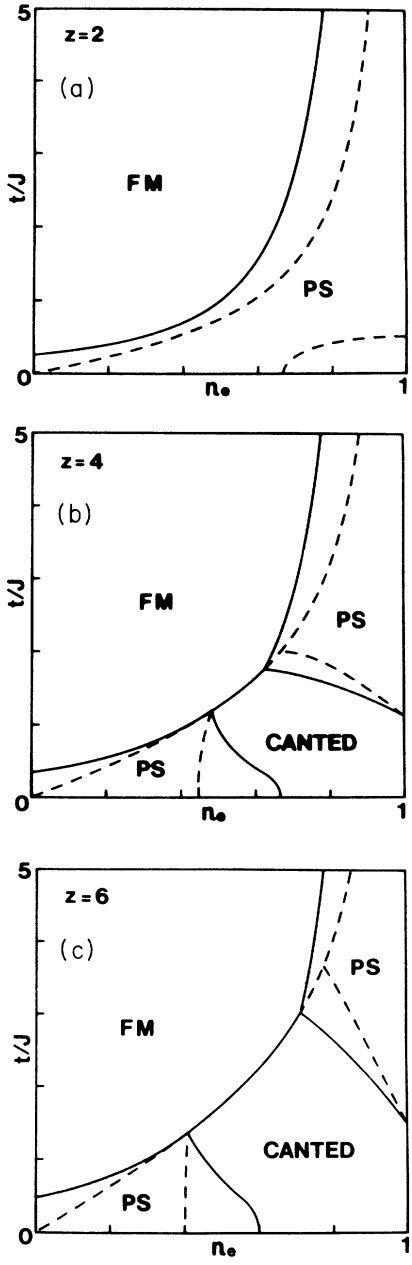

FIG. 4. $T=0$ phase diagram, including the effects of the three-site Hamiltonian $\mathcal{H}_3$, for various coordination numbers ($z=2$, 4, and 6). The dashed lines represent limits of metastability defined by Eqs. (3.22) and (3.24). The solid lines are the true critical lines obtained with the geometrical construction explained in the text. In addition to the uniform ferromagnetic phase (FM), a uniform canted phase is possible for lattice dimension greater than one ($z>2$). Phase separation (PS) occurs in the remaining regions of the phase diagram.

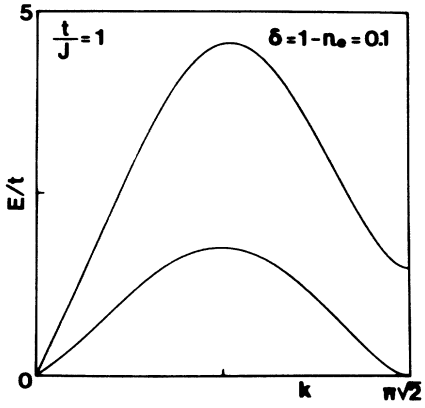

FIG. 5. Spectrum of elementary excitations in the uniform canted phase on a square lattice, including the effects of $\mathcal{H}_3$. The excitation energy E is plotted as a function of the crystal momentum k along the diagonal of the Brillouin zone. Both the magnon (upper curve) and the holon (lower curve) excitation energies are linear functions of the momentum near the zone center.

As an example, consider a square lattice in two dimensions ($z=4$) and a value of t/J in the vicinity of unity, a situation thought to be relevant for the study of copper oxide superconductors. Figure 4 suggests that the canted phase is stable for, say, $t/J=1$, and small doping. For slightly larger values of t/J, phase separation occurs where canted domains form within an antiferromagnetic background; these are reminiscent of the spin bags of "reduced antiferromagnetic order" advocated in Ref. 9. One should also mention that some experimental evidence for a canted phase has recently become available.[14] The model and methodology presented in this paper provide a vehicle for a more detailed study of these issues. For instance, we present in Fig. 5 our results for the spectrum of elementary excitations in the uniform-canted phase. An important feature of this figure is that the holon mode is no longer vanishing. The spectrum is more involved in a phase-separated system because of the appearance of additional (surface) modes due to the interface.

IV. ONE-DIMENSIONAL CLASSICAL MODEL

The main technical problem encountered in this work is the minimization of the classical energy (3.1). Our heuristic analysis of Sec. III produced a picture of phase separation that was confirmed to some extent by numerical experiments. Yet most of these experiments were based on the somewhat restricted form of the classical energy given in (3.4) which assumes a planar spin configuration, and makes a local phase factor ψ_l uniform. One may question whether or not the energy can be lowered even further by relaxing these assumptions.

We do not have a completely satisfactory answer to this question, except in the one-dimensional model which we discuss in this section. Of course, the quantum model is not expected to exhibit phase separation in one dimension, as discussed in Sec. III. On the other hand, the

one-dimensional classical model does display phase separation at $T=0$ and can be used to illustrate the main point of this work with complete mathematical rigor.

Thus our main task in this section is to find the minimum of the classical energy (3.1) or (3.2) restricted to a one-dimensional lattice. At first sight, this problem appears to be just as intractable as in higher dimensions. Nonetheless, a complete answer is possible through a transfer-matrix technique. The strategy followed here is somewhat circuitous in that we will calculate the classical ground-state energy as the $T\rightarrow 0$ limit of the classical free energy. The latter is obtained from the classical partition function defined in Eq. (2.12). Throughout this section, we will again neglect the contribution from the three-site Hamiltonian $\mathcal{H}_3$.

In the initial stages of the calculation, we follow the well-known procedure used by Fisher for the solution of the classical Heisenberg model.[15] Hence we work with an open chain with Λ sites, so the partition function is written as

$$Z_{\rm cl}=\int \prod_{l=1}^{\Lambda} (d^2\zeta_l)T(\zeta_1,\zeta_2)T(\zeta_2,\zeta_3)\cdots T(\zeta_{\Lambda-1},\zeta_\Lambda) , \tag{4.1}$$

where the transfer matrix $T(\zeta_i,\zeta_j)$ is given by

$$T(\zeta_i,\zeta_j)=\exp\left\{-\beta\left[E_{ij}-\mu\left[\frac{n_i+n_j}{2}-n_e\right]\right]\right\} . \tag{4.2}$$

Here E_{ij} is the expression under the summation sign in the classical energy (3.1) or (3.2) and μ is the chemical potential. We can exploit the rotational invariance of the energy to perform the angular integrations in (4.1) by a procedure similar to Fisher's original calculation.[15] Equation (4.1) becomes

$$Z_{\rm cl}=\text{const}\int_0^1 \prod_l (n_l dn_l)\tau(n_1,n_2) \times\tau(n_2,n_3)\cdots\tau(n_{\Lambda-1},n_\Lambda) , \tag{4.3}$$

where the reduced transfer matrix τ is given by

$$\tau(n_i,n_j)=e^{\beta c}\int_0^\pi d\theta\sin\theta I_0\left[\beta a\cos\frac{\theta}{2}\right]e^{\beta b(1-\cos\theta)} , \tag{4.4a}$$

with

$$a=2t[n_i(1-n_i)n_j(1-n_j)]^{1/2} , \quad b=\tfrac{1}{4}Jn_in_j, \quad c=\mu\left[\frac{n_i+n_j}{2}-n_e\right] . \tag{4.4b}$$

The function I_0 is the modified Bessel function. The overall multiplicative factor in Eq. (4.3) is not essential for the ensuing arguments and will be dropped for notational simplicity.

Although the derived effective theory in terms of charge density remains difficult to solve analytically, a significant reduction of degrees of freedom has been achieved. We are thus able to study the effective theory rather efficiently, using both numerical and analytical methods. The classical partition function (4.3) can be expressed in terms of the eigenvalues λ of the integral equation

$$\int_0^1 n'dn'\tau(n,n')f(n')=\lambda f(n) . \tag{4.5}$$

Actually, this equation applies to a periodic chain,[16] rather than to the open chain used in our earlier argument, but this distinction becomes unimportant in the thermodynamic limit ($\Lambda\rightarrow\infty$). In this limit, the partition function is given by $Z_{\rm cl}\approx\lambda_0^\Lambda$, where λ_0 is the largest eigenvalue of (4.5), and the free energy by $F_{\rm cl}/\Lambda=-\beta^{-1}\ln\lambda_0$.

One may wonder how an integral equation such as (4.5), whose kernel depends on the variables of two sites only, could reproduce the picture of phase separation derived in Sec. III for the infinite system. Roughly speaking, contact with the infinite system is made through the chemical potential which appears in the kernel of (4.5). This claim is made more precise below.

Although it does not seem possible to solve the integral equation analytically, a numerical solution is possible for practically all temperatures. Furthermore, the low-temperature limit, which is the limit of present interest, can be worked out analytically. We first describe the results of a numerical solution of Eq. (4.5). It is convenient first to remove the explicit dependence of the kernel on the charge density n_e, which can be achieved by absorb-

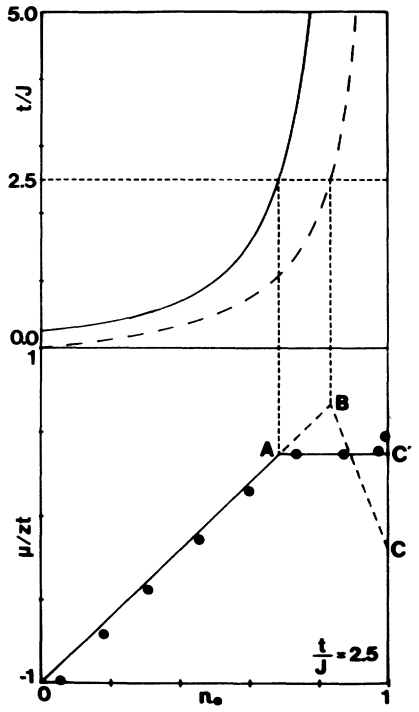

FIG. 6. The analog of the geometrical construction of Fig. 2, in terms of chemical potential instead of energy. The dots represent a numerical solution of the integral equation of Sec. IV at $2t\beta=100$.

ing n_e into the eigenvalue λ. The integral equation is written as

$$\int_0^1 n'dn'\kappa(n,n')f(n')=\nu f(n) ,$$
$$\kappa(n,n')=e^{\beta\mu n_e}\tau(n,n'), \quad \nu=e^{\beta\mu n_e}\lambda , \tag{4.6}$$

and the free energy is given by

$$F_{\rm cl}/\Lambda=-\beta^{-1}\ln\nu_0+\mu n_e , \tag{4.7}$$

where ν_0 is the largest eigenvalue of (4.6). Since the kernel of (4.6) depends on the charge density n_e only through the chemical potential, one may treat the latter as the independent variable. Once a solution of (4.6) is obtained for a specific value of μ, the corresponding density is calculated from

$$n_e=\frac{\int_0^1 dn\, n^2f^2(n)}{\int_0^1 dn\, nf^2(n)}=n_e(\mu) . \tag{4.8}$$

The relationship between n_e and μ turns out to be one to one, so Eq. (4.8) may be inverted without difficulty to yield $\mu=\mu(n_e)$.

A numerical solution of the integral equation is now straightforward and yields the free energy through Eq. (4.7), as a function of temperature and charge density. Here we concentrate on the low-temperature region ($\beta\to\infty$) where the free energy is expected to reduce to the sought after minimum of the classical energy. It is instructive to present the main result in terms of the chemical potential $\mu=\mu(n_e,\beta)$. Numerical data obtained for $t/J=2.5$ and $2t\beta=100$ are represented by dots in Fig. 6. This figure is the analog of Fig. 2, which was described in Sec. III, depicting the chemical potential instead of the energy. The solid line in the lower half of the figure is the chemical potential of the phase-separated solution (3.19), whereas the dashed line corresponds to the uniform solution (3.9). It is clear that the numerical data approach the solution corresponding to phase separation, a result that we reproduced for many different values of t/J. The small deviations from (3.19) are due to the finiteness of $T=1/\beta$. Strictly speaking, phase separation occurs only at $T=0$ in this one-dimensional model. Finally, we note the obvious fact that the corresponding numerical data for the free energy approach the ground-state energy of (3.18).

We now turn to an analytical explanation of the numerical data described above. An asymptotic expression for the transfer matrix defined in Eqs. (4.4) and (4.6) is given by

$$\kappa(n,n')\sim e^{-\beta g(n,n')}, \quad \text{for } \beta\to\infty , \tag{4.9a}$$

where

$$g(n,n')\equiv\epsilon(n,n')-\frac{\mu}{2}(n+n') ,$$

$$\epsilon(n,n')=2t\begin{cases}-\frac{t}{J}(1-n)(1-n')-\frac{J}{4t}nn', & \text{for } \frac{t}{J}\le\frac{1}{2}\left[\frac{nn'}{(1-n)(1-n')}\right]^{1/2};\\ -[n(1-n)n'(1-n')]^{1/2}, & \text{for } \frac{t}{J}\ge\frac{1}{2}\left[\frac{nn'}{(1-n)(1-n')}\right]^{1/2}.\end{cases} \tag{4.9b}$$

Here we neglect prefactors and other subleading contributions in the limit $\beta\to\infty$. An interesting feature of the effective energy $\epsilon(n,n')$ in Eq. (4.9b) is that it reduces to the energy of the uniform phase, found earlier in Eq. (3.8), when $n=n_e=n'$.

In the low-temperature limit, solutions of the integral equation are peaked around the stationary points of the approximate kernel (4.9), which are the minima of the function $g(n,n')$. It turns out that the extrema of $g(n,n')$ are symmetric under exchange of n and n', so we may work with the restricted function

$$g(n,n)=2t\begin{cases}-\frac{t}{J}(1-n)^2-\frac{J}{4t}n^2-\bar{\mu}n, & \text{for } \frac{t}{J}\le\frac{n}{2(1-n)},\\ -n(1-n)-\bar{\mu}n, & \text{for } \frac{t}{J}\ge\frac{n}{2(1-n)} ,\end{cases} \tag{4.10}$$

where $\bar{\mu}=\mu/2t$. For a given value of the reduced chemical potential $\bar{\mu}$, the function (4.10) develops either a local minimum in the region $t/J\ge n/2(1-n)$;

$$n=n_0=\frac{1+\bar{\mu}}{2} ,$$
$$g(n_0,n_0)=-2t[\tfrac{1}{4}(1-\bar{\mu}^2)+\tfrac{1}{2}\bar{\mu}(1+\bar{\mu})] , \tag{4.11}$$

or a local maximum in the region $t/J\le n/2(1-n)$. The latter is not relevant for the asymptotic analysis. However, there is also an endpoint minimum which is present for all values of t/J;

$$n=1, \quad g(1,1)=-2t\left[\frac{J}{4t}+\bar{\mu}\right] . \tag{4.12}$$

For sufficiently small values of $\bar{\mu}$, the minimum (4.11) is dominant and leads to the ferromagnetic solution in the limit $\beta\to\infty$. In particular, since f becomes sharply peaked about n_0, Eq. (4.8) yields $n_e\approx n_0=(1+\bar{\mu})/2$, or $\bar{\mu}\approx 2n_e-1$, which is the expected linear dependence depicted in Fig. 6 and found previously in (3.19). One might expect that this solution remains in force until the inequality $t/J\ge n_e/2(1-n_e)$ is saturated. In fact, the inequality is never saturated because the endpoint minimum (4.12) becomes dominant at an earlier stage. The critical value of $\bar{\mu}$ at which (4.12) becomes the lower minimum is given by the solution of the algebraic equation

$$g(n_0,n_0)=g(1,1)\Longrightarrow\bar{\mu}=\bar{\mu}_c=1-\left[\frac{J}{t}\right]^{1/2}, \quad (4.13)$$

again in agreement with Eq. (3.19), recalling that $\bar{\mu}=\mu/2t$. For large but finite β, $\bar{\mu}$ rises almost linearly as a function of density until it reaches the critical value $\bar{\mu}_c$ at which the two minima (4.11) and (4.12) become degenerate. A small further increase of $\bar{\mu}$ beyond $\bar{\mu}_c$ rapidly shifts the wave function $f(n)$ from the ferromagnetic minimum (4.11) to the endpoint minimum (4.12). Thus small variations of $\bar{\mu}$ cause a rapid variation of the average density between the ferromagnetic value $n=(1+\bar{\mu})/2$ and the endpoint value $n=1$. This explains the plateau in the data of Fig. 6; and in the strict limit $\beta\rightarrow\infty$, this analysis reproduces the results of Sec. III.

Using standard asymptotic methods, one could carry the preceding analysis further and compute explicitly the behavior of the chemical potential and the free energy in the preasymptotic region $T\sim 0$. However, these finer details are not relevant for the main point of this section, which was to establish rigorously that the minimum of the classical energy is indeed the one obtained by heuristic methods in Sec. III.

Furthermore, the expression for $\epsilon(n,n')$ obtained in Eq. (4.9) may be used to write down an effective theory at low temperatures governed by the energy

$$E_{\text{eff}}=\sum_l\left[\epsilon(n_l,n_{l+1})-\mu(n_l-n_e)\right], \quad (4.14)$$

where we have included the global constraint. Of course, angular degrees of freedom do not appear in (4.14), but their effect has correctly been accounted for in $\epsilon(n,n')$.

Because of the absence of explicit angular degrees of freedom in (4.14), a numerical minimization of the effective energy is now practical for long chains ($\Lambda\sim 1000$). In this way, not only have we verified again the presence of phase separation for densities in the region

$$n_-\le n_e\le 1;\quad n_-=1-\frac{1}{2}\left[\frac{J}{t}\right]^{1/2}, \quad (4.15)$$

but we have also obtained detailed information about the nature of the interface. The result of a typical calculation is sketched in Fig. 7, which plots density as a function of distance in a solid line to illustrate the formation of a kink at the interface. Beneath the curve for the density, we have supplied the direction of the spins in accord with our analysis of Sec. III. The interface is microscopically sharp on the antiferromagnetic side, but develops an exponential tail on the ferromagnetic side.

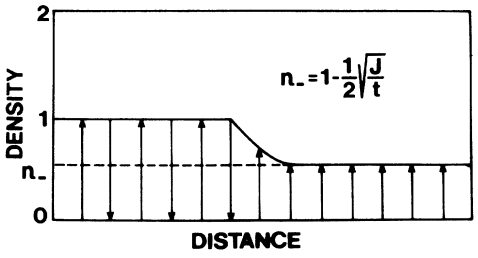

FIG. 7. Sketch of the interface in the one-dimensional classical model. The interface is sharp on the antiferromagnetic side, but develops an exponential tail on the ferromagnetic side.

Analytical understanding of the interface is also possible by working out the difference equations resulting from a variation of the effective energy (4.14). These are unwieldy, due to the various regions one must consider in (4.9b), so we will not write them out here. For a typical density in the region (4.15), the asymptotic tail on the ferromagnetic side is described by

$$n_l\approx n_-+\text{const}\times e^{-l/\xi}, \quad (4.16)$$

where the correlation length ξ is given by

$$\cosh(1/\xi)=\frac{1}{\bar{\mu}^2}=\frac{1}{[1-(J/t)^{1/2}]^2}. \quad (4.17)$$

The correlation length vanishes in the special case $t/J=1$, which corresponds to vanishing chemical potential. A more detailed examination of the difference equations in this special case established that the interface consists of exactly one site, and that the explicit solution is given by

$$\frac{t}{J}=1;\quad n_l=\begin{cases}1 & \text{for } l<l_0,\\ \frac{1}{2}(1+5^{-1/2}) & \text{for } l=l_0,\\ n_-=\frac{1}{2} & \text{for } l>l_0.\end{cases} \quad (4.18)$$

This special solution could be used to illustrate the formation of surface modes alluded to at the end of Sec. III, but the task is beyond the scope of this paper.

V. CONCLUDING REMARKS

In the bulk of this paper, we have been faithful to the model defined in the introduction, trying to understand basic features of its phase diagram. The extent to which we have succeeded has already been debated in the main text. So we will assume that our solution of the model is correct, and attempt to draw some more general conclusions.

First, we will return to the partial bosonization incorporated in the commutation relations (1.6). Although we cannot gauge at this point the full effect of this simplification, we should re-emphasize that our model does share with the usual t-J model many essential physical characteristics. In particular, Nagaoka's arguments go through without modification. Thus our conclusions concerning the true ferromagnetic boundary should have impact on the corresponding question in the usual t-J model as well as in the Hubbard model.

Second, one must question whether a t-J model of any kind is an appropriate description of the Hubbard model. Recall that the t-J model is derived as the large-U limit of the Hubbard model, the limit being taken at any fixed electron density. Hence, if a ferromagnetic boundary actually exists, the limit would have to be taken through a phase boundary. Thus it is not obvious that the details of the phase diagram below the ferromagnetic boundary coincide with those of the original Hubbard model. Of course this criticism need not apply in low dimensions,

e.g., $D=1$, where the phase diagram of the quantum model is known to be featureless.

Let us assume for the sake of argument that the potential pitfalls described above prove harmless, and that phase separation is indeed predicted by the Hubbard model.[5,6] One should then question whether or not phase separation is generic; in particular, whether this picture is stable against variations of the Hubbard Hamiltonian. One worrisome objection is that we have described macroscopic aggregation of charge without considering the long-range effects of Coulomb repulsion. Coulomb repulsion may limit the growth of phase-separating bubbles, or else screening may allow them to grow to arbitrary size. In the latter case, one contemplates the important effects of screening charges which until now have not even been included in the problem. Either scenario suggests that phase separation may push the Hubbard model beyond its limit of applicability. Such a conclusion could prove disastrous not only for potential applications of the simple Hubbard model to high-T_c superconductivity, but also for more conventional applications to metallic magnetism.

ACKNOWLEDGMENTS

This work was supported in part by a research grant from the E.E.C. (ESPRIT-3041). The work of N.P. was also supported by the U.S. Department of Energy, while G.C.P. acknowledges support also from the Greek Secretariat for Science and Technology (Contract No. 87ED215). M.P.M. is grateful to the members of the Research Center of Crete for welcoming him to join their work during his summer on Crete. We thank E. N. Economou, P. Spathis, and L. Kleinman for valuable discussions.

---

*Present address: Center for Nonlinear Dynamics, and Department of Physics, University of Texas, Austin, TX 78712.

†Also at the Department of Physics, Washington University, St. Louis, MO 63130.

[1]E. H. Lieb and F. Y. Wu, Phys. Rev. Lett. **20**, 1445 (1968).

[2]Y. Nagaoka, Phys. Rev. **147**, 392 (1966).

[3]A. B. Harris and R. V. Lange, Phys. Rev. **157**, 295 (1967).

[4]N. Papanicolaou, Nucl. Phys. **B240**, 281 (1984); **305**, 386 (1988).

[5]P. B. Visscher, Phys. Rev. B **10**, 943 (1974).

[6]L. B. Ioffe and A. I. Larkin, Phys. Rev. B **37**, 5730 (1988).

[7]D. Foerster, Z. Phys. B **74**, 295 (1989).

[8]W. F. Brinkman and T. M. Rice, Phys. Rev. B **2**, 1324 (1970).

[9]J. R. Schrieffer, X.-G. Wen, and S.-C. Zhang, Phys. Rev. Lett. **60**, 944 (1988).

[10]G. C. Psaltakis, Phys. Rev. B **39**, 2834 (1989).

[11]J. C. Maxwell, Nature **11**, 53 (1874); also in *Collected Works*, edited by W. D. Niven (Dover, New York, 1952), Vol. 2, p. 424; J. W. Gibbs, Trans. Conn. Acad. Arts Sci. **3**, 108 (1878); also in *The Scientific Papers of J. W. Gibbs*, edited by H. A. Bumstead and R. G. Van Name (Dover, New York, 1961).

[12]S. Tang and J. E. Hirsch, Phys. Rev. B **39**, 4548 (1989).

[13]H. Shiba, Phys. Rev. B **6**, 930 (1972).

[14]Tineke Thio *et al.*, Phys. Rev. B **38**, 905 (1988).

[15]M. E. Fisher, Am. J. Phys. **32**, 343 (1964).

[16]G. S. Joyce, Phys. Rev. **155**, 478 (1967).